Geophys. J. Int. (1995) **123**, 161–168

Subspace inversion of electromagnetic data: application to mid-ocean-ridge exploration

Martyn Unsworth* and Doug Oldenburg
Department of Geophysics and Astronomy, University of British Columbia, Vancouver, BC, Canada, V6T 1Z4

Accepted 1995 April 25. Received 1995 April 10; in original form 1994 October 24

SUMMARY

Controlled-source electromagnetic (CSEM) surveys have the ability to provide tomographic images of electrical conductivity within the Earth. The interpretation of such data sets has long been hampered by inadequate modelling and inversion techniques. In this paper, a subspace inversion technique is described that allows electric dipole–dipole data to be inverted for a 2-D electrical conductivity model more efficiently than with existing techniques. The subspace technique is validated by comparison with conventional inversion methods and by inverting data collected over the East Pacific Rise in 1989. A model study indicates that, with adequate data, a variety of possible mid-ocean-ridge conductivity models could be distinguished on the basis of a CSEM survey.

Key words: electrical conductivity, electromagnetic surveys, inversion, mid-ocean ridge, subspace.

1 INTRODUCTION

The ability of electromagnetic survey techniques to image Earth structure has improved significantly in recent years. This has been primarily due to advances in modelling and inversion techniques as well as increased computer power, and we are now approaching the point where realistic geologic complexity can be emulated with numerical models. The greatest impediments to inversion are the inability to represent the Earth in a model with very fine cellurization, and also the inherent non-uniqueness of the inversion result. Despite these limitations, inversion results can provide valuable information about the conductivity distribution in the Earth.

The magnetotelluric (MT) inverse problem was one of the first to be satisfactorily solved [see Whittall & Oldenburg (1992) for a review]. This is because the forward modelling is comparatively simple, due to the 1-D plane-wave source fields. MT data sets are now routinely inverted for a 2-D conductivity structure (Smith & Booker 1988; deGroot Hedlin & Constable 1990). However the 3-D source fields generated by a dipole source make the modelling and inversion of controlled-source electromagnetic (CSEM) data a much more involved task. Although, in principle, existing inversion methodologies can be extended to higher dimensions, the increased computational cost can prohibit implementation, as is clear from the small number of solutions that have been published. Oristaglio & Worthington (1980) presented the results of inverting CSEM data from an infinitely long wire over a dike-shaped ore body and showed that inversion of the surface fields defined the location of the body. However, limitations in computer memory meant they could not finely parametrize their model, or consider the finite nature of a realistic source. More recently, a number of authors have considered the inversion of EM data acquired in a cross-borehole configuration. Newman (1992) used an integral equation approach and inverted for a 2-D conductivity model. Torres-Verdin & Habashy (1993) used a Born scattering approach to recover a 2-D conductivity structure located between two boreholes. Lee & Xie (1993) described a novel approach in which the diffusive electromagnetic fields are transformed into a domain in which they have the properties of waves. This allows the principles of seismic tomography to be used in the inversion.

In this paper we report on an inversion method for dipole–dipole CSEM experiments with both transmitters and receivers located on the ocean floor. The earth model is 2-D but the transmitter and receiver dipoles are 3-D, so the method is referred to as $2\frac{1}{2}$-D. The paper begins with an outline of the theory behind the forward modelling and inversion methodologies, and the features that have reduced the computational costs are emphasized. The utility of the method is then demonstrated by a model study of a CSEM survey of a mid-ocean ridge.

* Now at: Geophysics Program, AK-50, University of Washington, Seattle, WA 98195, USA.

2 THEORY

2.1 Inversion methodology

In a general inverse problem, such as obtaining a conductivity model of the Earth from surface observations of electromagnetic fields, we are provided with N data, $d_j^{\rm obs}$, some estimate of their uncertainties, ε_j, and mappings of a form which expresses the relationship between the jth datum d_j and a model $\mathbf{m}$, which in our case will be the logarithm of electrical conductivity. The goal is to recover an $\mathbf{m}$ which adequately reproduces the observations and at the same time has desirable attributes so as to facilitate geophysical interpretation of the conductivity. The primary difficulty in solving the inverse problem lies in the non-uniqueness of the solution. Accordingly, a practical and common inversion methodology is to introduce an objective function $\Phi_m(m)$ and a data misfit functional $\Phi_d(m)$ and solve the inversion problem by finding that $\mathbf{m}$ which minimizes Φ_m subject to the restriction that $\Phi_d=\Phi_d^*$, where Φ_d^* is a desired target value for the misfit functional. We are thus lead to minimizing $\Phi(m)=\Phi_m+\mu(\Phi_d-\Phi_d^*)$ where μ is a Lagrange multiplier.

To proceed numerically for the 2-D inverse problem, we divide the earth into a set of M rectangular cells and let m_j denote the constant value of log conductivity of the jth cell. The model objective function is the discretized version of

$$\Phi_m(m)=\alpha_s\int_{\rm area} w_s(m-m_0)^2\,ds + \alpha_y\int_{\rm area} w_y\frac{\partial(m-m_0)^2}{\partial y}ds + \alpha_2\int_{\rm area} w_z\frac{\partial(m-m_0)^2}{\partial z}ds, \tag{1}$$

and is written as

$$\Phi_m(\mathbf{m})=(\mathbf{m}-\mathbf{m}_0)^{\rm T}(\alpha_s\mathbf{W}_s^{\rm T}\mathbf{W}_s+\alpha_x\mathbf{W}_x^{\rm T}\mathbf{W}_x+\alpha_z\mathbf{W}_z^{\rm T}\mathbf{W}_z)\times(\mathbf{m}-\mathbf{m}_0) = |\mathbf{W}_m(\mathbf{m}-\mathbf{m}_0)|^2, \tag{2}$$

where $\mathbf{W}_s$, $\mathbf{W}_x$ and $\mathbf{W}_z$ are $M\times M$ matrices. In eq. (1) the constant α_s controls the importance of closeness of the constructed model to the reference model $\mathbf{m}_0$, and α_x and α_z control the roughness of the model in both spatial directions. The reference model can be omitted from the derivatives terms in eq. (1) if desired. With the same model parametrization, the forward mapping is written as $\mathbf{d}=\mathscr{F}(\mathbf{m})$. Let the data misfit functional be

$$\Phi_d=|\mathbf{W}_d(\mathbf{d}-\mathbf{d}^{\rm obs})|^2, \tag{3}$$

where $\mathbf{W}_d$ is an $N\times N$ data weighting matrix. For this paper we shall assume that the noise contaminating the jth observation is an uncorrelated Gaussian random variable having zero mean and standard deviation ε_j. Correspondingly, Φ_d is the chi-squared variable with N degrees of freedom.

Our inversion problem is solved by finding the model $\mathbf{m}$ and the Lagrange muliplier μ such that the objective function

$$\Phi(\mathbf{m})=\phi_m(\mathbf{m})+\mu^{-1}[\phi_d(\mathbf{d})-\phi_d^*] \tag{4}$$

is minimized, where ϕ is the global misfit. The problem is nonlinear and so iteration is required. Let $\mathbf{m}^{(n)}$ be the model at the nth iteration and let $\mathbf{d}^{(n)}$ denote the predicted data. We search for a perturbation $\delta\mathbf{m}$ which reduces Φ. Performing a first-order Taylor expansion of the data about $\mathbf{m}^{(n)}$ yields

$$\mathbf{d}(\mathbf{m}^{(n)}+\delta\mathbf{m})=\mathbf{d}^{(n)}+\mathbf{J}\delta\mathbf{m}, \tag{5}$$

where the $N\times M$ sensitivity matrix $\mathbf{J}$ has elements $J_{ij}=\partial d_i/\partial m_j$. The perturbed objective function is

$$\phi(\mathbf{m}^{(n)}+\delta\mathbf{m})=|W_m(\mathbf{m}^{(n)}+\delta\mathbf{m}-\mathbf{m}_0)|^2 + \mu^{-1}[|\mathbf{W}_d(\mathbf{d}^{(n)}+\mathbf{J}\delta\mathbf{m}-\mathbf{d}^{\rm obs})|^2-\phi_d^*]. \tag{6}$$

The details of how to compute the sensitivity elements J_{ij} for the $2\frac{1}{2}$-D problem considered here are given in Appendix A.

Minimization of eq. (6) with respect to the variable $\delta\mathbf{m}$ yields an $M\times M$ system of equations to be solved. For the problems considered here, where M is typically 1000 or more, we reduce the number of computations by employing a subspace technique (Skilling & Bryan 1984; Kennett & Williamson 1988; Oldenburg, McGillivray & Ellis 1993). Let $\mathbf{m}^{(n)}$ be the model at the nth iteration and let $\mathbf{v}_i$, $i=1,q$ be arbitrary vectors which form a q-dimensional subspace of R^M. We seek a model perturbation of the form $\delta\mathbf{m}=\Sigma\,\alpha_i\mathbf{v}_i=\mathbf{V}\alpha$. Substituting this into eq. (6) yields

$$\phi(\alpha)=|\mathbf{W}_m(\mathbf{m}^{(n)}+\mathbf{V}\alpha-\mathbf{m}_0)|^2 + \mu^{-1}[|\mathbf{W}_d(\mathbf{d}^{(n)}+\mathbf{J}\mathbf{V}\alpha-\mathbf{d}^{\rm obs})|^2-\phi_d^*]. \tag{7}$$

Setting $\nabla_\alpha\phi(\alpha)=0$ yields

$$\mathbf{B}\alpha=\mathbf{b}, \tag{8}$$

where

$$\mathbf{B}=\mathbf{V}^{\rm T}(\mathbf{J}^{\rm T}\mathbf{W}_d^{\rm T}\mathbf{W}_d\mathbf{J}+\mu\mathbf{W}_m^{\rm T}\mathbf{W}_m)\mathbf{V} \tag{9}$$

and

$$\mathbf{b}=-\mu\mathbf{V}^{\rm T}\mathbf{W}_m^{\rm T}\mathbf{W}_m(\mathbf{m}^{(n)}-\mathbf{m}_0) - \mathbf{V}^{\rm T}\mathbf{J}^{\rm T}\mathbf{W}_d^{\rm T}\mathbf{W}_d(\mathbf{d}^{(n)}-\mathbf{d}^{\rm obs}). \tag{10}$$

The matrix $\mathbf{B}$ is a $q\times q$ positive definite and symmetric matrix, and is easily inverted provided that q is relatively small.

The success of the subspace method clearly lies in the choice of vectors. As in Oldenburg *et al.* (1993) we choose vectors that are obtained by segmenting Φ_d and Φ_m, computing associated gradient directions, and converting these to steepest-descent vectors by multiplying by $(\mathbf{W}_m^{\rm T}\mathbf{W}_m)^{-1}$. For this paper we have generally grouped the data according to frequency, and then had one vector associated with amplitudes and one with phases. We have also used vectors which corresponded to rows of our model. This facilitates the recovery of layered earth models. The inversion algorithm starts with an initial conductivity model, and in each iteration this is updated by $\delta\mathbf{m}$ until the model fits the data and is as smooth as possible.

In the following section we present examples using various choices of basic functions, and compare the results to those obtained via the more conventional method of solving directly for a conductivity perturbation in each cell.

2.2 Forward modelling

The inversion algorithm is written so as to minimize the number of forward modellings per iteration. Even so, the algorithm used for forward modelling should be as fast as possible, as well as being accurate (it should be accurate to a higher degree than the standard errors of the data being inverted). Throughout this study, the $2\frac{1}{2}$-D finite-element code developed by Unsworth, Travis & Chave (1993) has been used. This computes the electromagnetic response of a 2-D earth to the electromagnetic fields of a dipole transmitter by reducing the 3-D problem to a set of 2-D ones by a Fourier transform. The code uses a combination of infinite elements and an iterative solution to reduce computation time and memory requirements. The iterative solution is particularly effective in an inversion when the electromagnetic fields are being computed for a set of generally similar conductivity structures. The first forward modelling starts the iteration with the fields set to zero. As the inversion proceeds and the conductivity model is updated, the iteration begins with the electromagnetic fields from the previous conductivity model. This results in a significant saving in computation time. The efficient calculation of sensitivities is also a key part of inversion. We calculate the sensitivities exactly, using the adjoint method described by McGillivray, Oldenburg & Ellis (1994), and the calculation is described in Appendix A.

3 VALIDATION OF CODE

3.1 Sea-floor example

Logistical problems apart, the ocean floor is an excellent place to use controlled-source electromagnetic techniques. The conductive ocean layer screens out high-frequency noise and produces an electrically quiet environment in which weak signals may be detected. The electrical conductivity contrast between the sea-water and the sea-floor ensures that electromagnetic energy detected more than a few ocean skin depths from the transmitter will have travelled through the sea-floor and be sensitive to its conductivity. Chave, Edwards & Constable (1990) give an overview of theory and instrumental considerations for sea-floor CSEM.

This example simulates a controlled-source electromagnetic survey on the ocean floor. It will be used to demonstrate how the choice of subspace vectors influences the final conductivity model produced by the inversion.

The electrical conductivity model used to generate synthetic data is shown in the upper left panel of Fig. 1. It represents a range of features with spatial scales and conductivities that might be found at a mid-ocean ridge, although the asymmetry does not imply that such ocean ridges are necessarily asymmetric. The model is overlain by a conductive half-space representing the ocean, with a conductivity of $3\,\mathrm{S\,m^{-1}}$ (this is not shown in the figure). On the right-hand side, the sea-floor has a uniform conductivity of $0.01\,\mathrm{S\,m^{-1}}$, and on the left it has a $0.01\,\mathrm{S\,m^{-1}}$ layer overlying a $0.001\,\mathrm{S\,m^{-1}}$ half-space. In the centre is a conductive prism ($0.3\,\mathrm{S\,m^{-1}}$), similar in size to that proposed for a mid-ocean-ridge magma chamber by Unsworth (1994).

Synthetic data were then generated by using a horizontal electric dipole at each of the 11 locations marked by 'x' in Fig. 1. The signals are recorded by receivers at the other 10 locations at frequencies of 8, 2 and 0.5 Hz. Both transmitter and receiver are oriented out of the plane of the paper. Each observation consists of a field strength and a phase measurement, giving a total of 660 data. The data are displayed in Fig. 2, and it can be seen that, when the transmitter is located in the centre of the model, the fields attenuate most rapidly over the conductive zone to the right. The synthetic data were then contaminated with 2 per cent Gaussian noise.

The data were then inverted using the subspace technique. The model **m** with which we attempt to reproduce the data has 798 cells, and the weighting matrix $\mathbf{W}_m$ was chosen to produce the smoothest model ($\alpha_s = 10^{-7}, \alpha_x = 1, \alpha_z = 1$). The first inversion used 28 subspace vectors consisting of 21 horizontal row vectors, one gradient vector of the model norm, ϕ_m, and six gradient vectors of the data misfit, subdivided by field strength, phase and frequency. The starting model was a uniform half-space with $\sigma = 0.01\,\mathrm{S\,m^{-1}}$, hence $\phi_m = 0$. The convergence is shown in Fig. 3. Initially, the data misfit decreases rapidly, down to a value of $\phi_d = 2.0$, but after this the convergence is much slower. The inversion converges at the 35th iteration with a data misfit $\Phi_d = 1.0$, and a model norm of $\Phi_m = 1.7$. The model norm slowly increases as structure is added to enable a model to be found that fits the data. The final conductivity is shown in the upper right panel of Fig. 1. The layered structure on the left is clearly imaged, as is the shape and conductivity of the conductive prism in the centre. Structure below 5 km is poorly imaged, and horizontal streaks of high conductivity at a depth of 1–2 km do not suggest that the smoothest possible model has been found with this set of vectors.

To see if a smoother model could be obtained by using more subspace vectors, a second inversion of the same synthetic data was performed using 88 subspace vectors. A set of 66 vectors was obtained by dividing the data misfit functional with respect to field strength, phase, frequency and transmitter location. The row vectors and model norm gradient vectors from the previous inversion were also used, producing a total of 88 subspace vectors. The convergence is shown in Fig. 3, and the desired misfit was achieved by the 7th iteration, but two more iterations were needed to smooth the model and reduce the model norm to a value of $\Phi_m = 1.5$. The final model has a lower model norm (i.e. it is smoother) than that obtained with 28 vectors. The final conductivity model is shown in the lower left panel of Fig. 1. The shallow structure is imaged as clearly as in the previous case, but below 3 km the original structure is more faithfully reproduced. The resistive zone on the left is more clearly resolved, but below 5 km the resolution is poor. This is principally due to the maximum transmitter–receiver offset being 12 km, and, with sensitivity limited to a depth of the order of half this value, we cannot expect to image clearly below this depth. Only signals diffusing from the transmitter at +6 km to a receiver at −6 km will sample the lowest part of the structure. The distribution of conductive or resistive structure along this energy path is non-unique, and the inversion simply produces the smoothest model that fits the data. The fit to the data is shown by the solid line in Fig. 2.

To demonstrate that the conductivity model obtained with 88 subspace vectors is not an artefact of the choice of subspace vectors, a final inversion was performed in which every cell was defined as a subspace vector (this is equivalent to not using the subspace approach at all). The convergence rate with these 798 vectors is shown in Fig. 3 and is indistinguishable from that with 88 vectors. The computation time, however, was increased by a factor of 5. This increase is not as dramatic as expected since a large proportion of the computation time is taken up with forward modelling, which does not depend on the number of subspace vectors used. The time spent on the inversion was increased by a factor of 20. The final

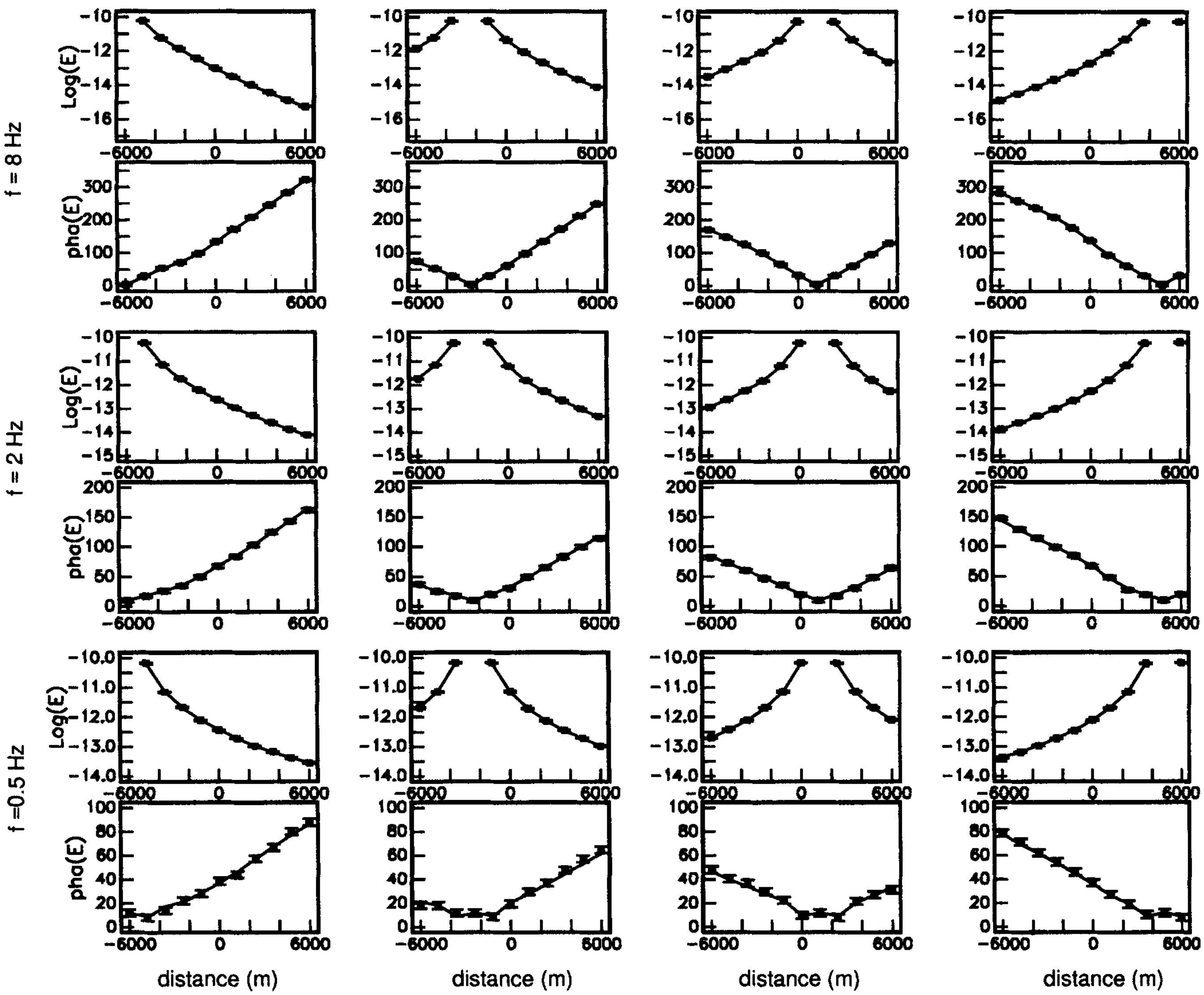

Figure 2. Synthetic data for the model shown in Fig. 1 with error bars. The solid lines show the fit to the data for the inversion with 2 per cent errors and 88 subspace vectors. For each profile the field strength (upper panel) is $\log_{10}$ of the electric field strength for a source with unit dipole moment. The phase of the electric field is in degrees, relative to the source. The four columns show data with the source located at -6000, -2400, 1200 and 4800 m, respectively.

conductivity model is shown in the lower right panel of Fig. 1, and is virtually identical to that obtained with just 88 subspace vectors. Thus inversions performed with the reduced set of 88 subspace vectors will image conductivity structure as effectively as the slow computation that uses 798 vectors.

3.2 Test on East Pacific Rise data

To date, no CSEM data sets have been acquired with sufficient data to constrain a 2-D conductivity structure. Hence the 2-D subspace inversion has been tested on 1-D controlled-source data collected in 1989 over the East Pacific Rise at 13°N. The analysis of these data is described by Evans *et al.* (1994), who binned the data by range and then used a regularized inversion to obtain a 1-D conductivity model. Since this binning effectively averages out any 2-D structure, the subspace inversion was required to produce a 1-D model, while still performing a fully $2\frac{1}{2}$-D forward modelling. Fig. 4 shows a comparison of the results for inversion of 8 Hz data collected over the ridge crest. The left-hand panel show the data (solid squares) with their standard errors and the response of the smoothest subspace conductivity model. The right-hand panel shows the conductivity models for the subspace inversion (solid line) and the 1-D inversion of Evans *et al.* (1994) (circles). Both models were required to be smooth in a first-derivative sense and can be seen to agree well. The minor differences that exist are due to the different parametrizations used in the two inversions.

4 MODEL STUDY OF MID-OCEAN-RIDGE (MOR) DATA

Unsworth (1994) considered the sensitivity of a controlled-source electromagnetic experiment to MOR structure on the basis of forward modelling, and showed that, providing the effects of near-surface conductivity variations were not extreme, various end-member conductivity models could be distin-

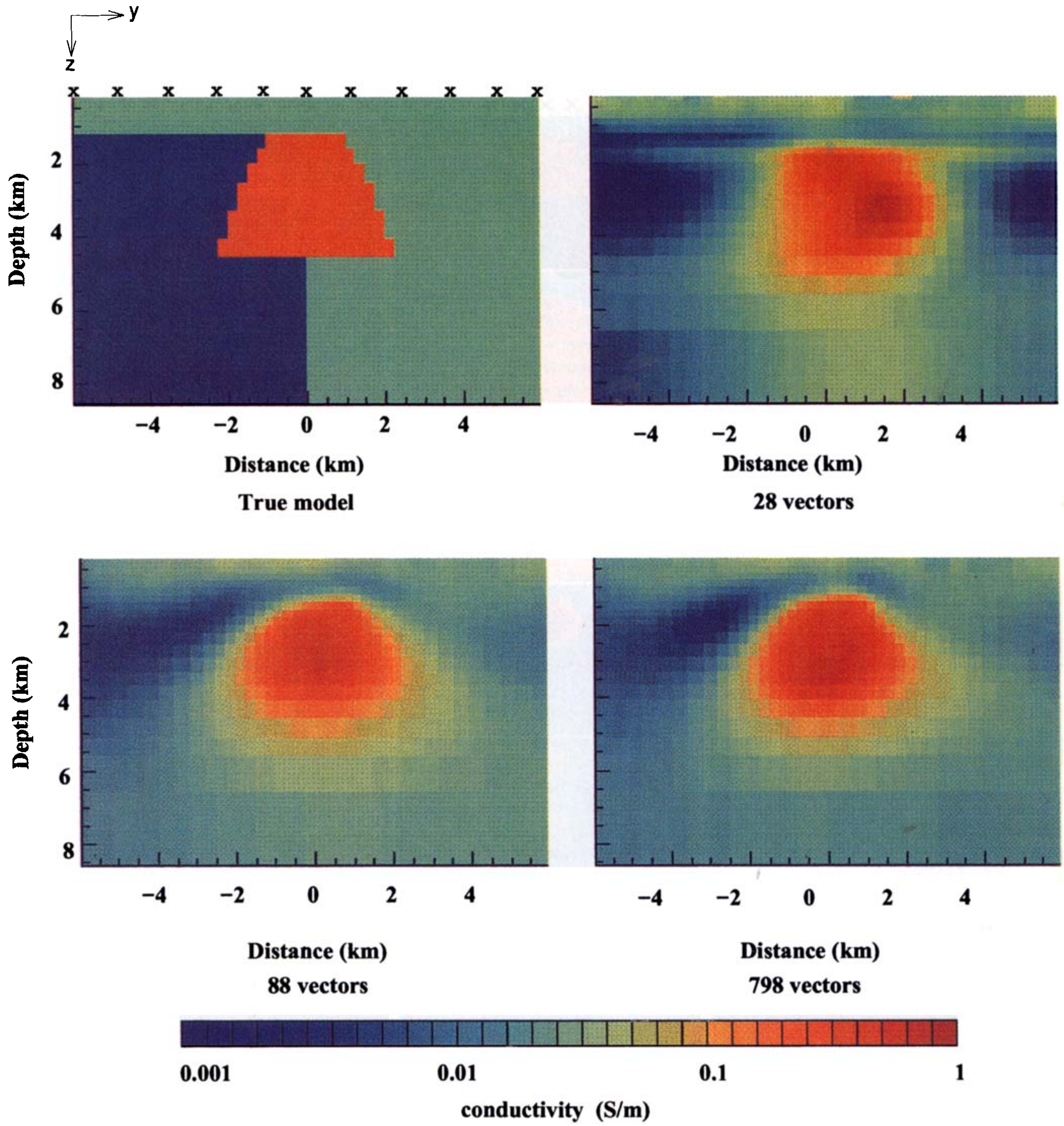

Figure 1. Inversion results for a sea-floor survey using a range of subspace vectors. The true conductivity model is shown in the upper left panel. The other panels show the inversion results when 2 per cent noise was added to the data. It can be seen that 28 vectors are inadequate to recover the information present in the data. 88 vectors produce a model almost indistinguishable from that with 798 vectors, but at a fraction of the computational cost.

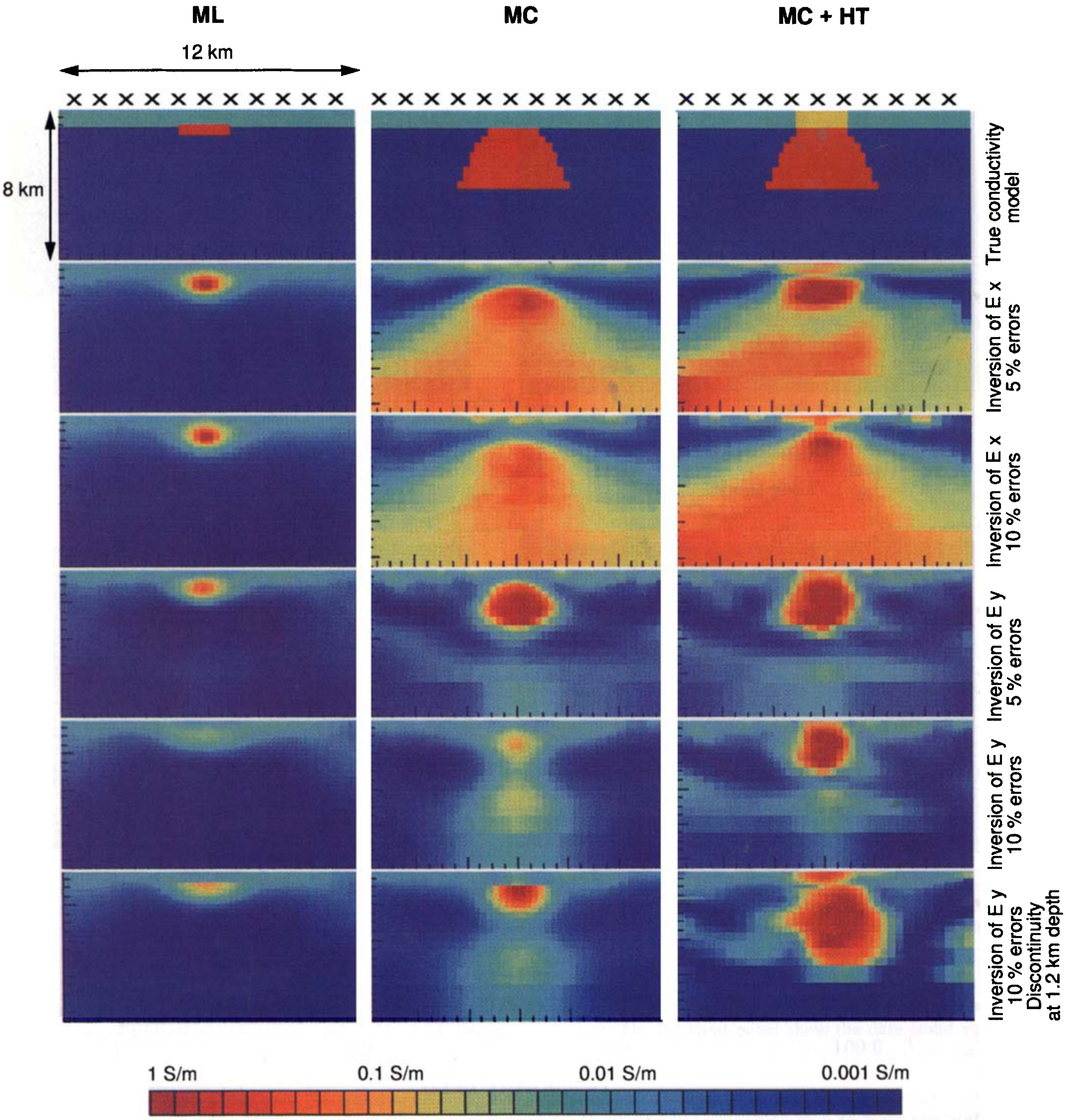

Figure 5. Electrical conductivity models for three possible MOR structures and the models obtained by inverting synthetic EM data at various noise levels. In each case field strength and phase data at 8, 2 and 0.5 Hz were inverted. All inversions start from a 0.01 S m^{-1} half-space. Instrument locations are marked by 'X'.

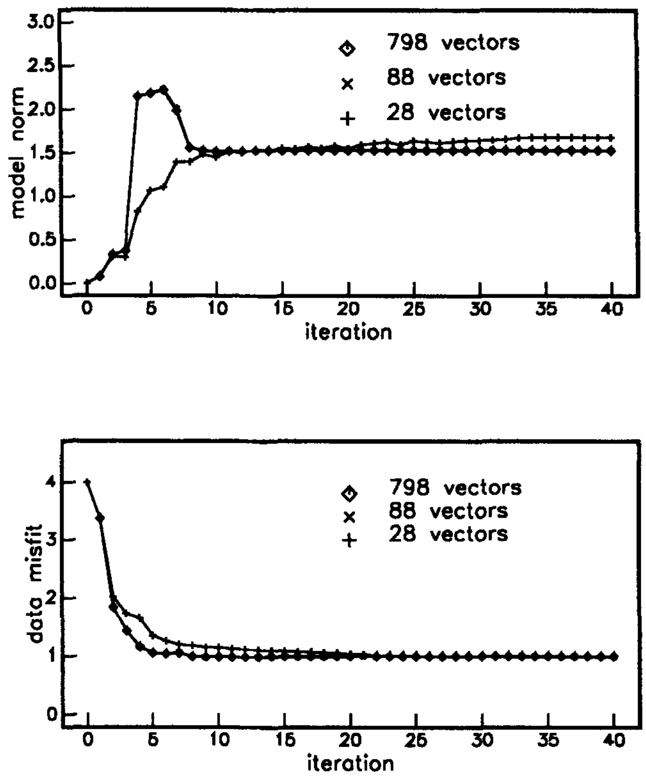

Figure 3. Model norm and normalized data misfit versus iteration number for inversion of symmetric data with 28, 88 and 798 subspace vectors.

guished. A more rigorous assessment of these experiments can be obtained by generating synthetic data, adding noise and then using an inversion algorithm. This approach can demonstrate whether certain features of the model can be recovered through inversion. This is superior to answering the same question by merely examining the forward modelled responses of the models and showing that they differ.

To compare the results of a theoretical inversion study with a real experiment, a number of factors must be borne in mind.

(1) The magnitude of the uncertainties/errors that are to be expected in the data must be estimated. Since very few CSEM ocean-bottom data sets exist, the magnitude of this quantity is very poorly constrained. Errors arise due to uncertainties in navigation and the location of receivers, as well as because of electrical noise present at the sea-floor. Topography and near-surface conductivity variations can spatially alias the data. While not strictly errors, these effects distort the data and limit the precision to which they can be interpreted. In the following section, the term 'errors' will be used to include both statistical errors and spatial aliasing. In locations with a relatively uniform sea-floor, errors in the range 5–25 per cent are possible [see experimental data of Evans *et al.* (1994) and the theoretical study by Unsworth (1994)]. However, in regions of rugged topography and very large horizontal variations of near-surface conductivity, these values could increase by several orders of magnitude. It is unlikely that a time-domain experiment would improve the situation. In both the time-domain (TD) and the frequency-domain (FD) surveys considered here, the magnitude of the electric field is the measurement most heavily distorted by near-surface structure. In both domains, the traveltime (TD) and the equivalent phase (FD) will be much less influenced by near-surface structure.

(2) The characteristics of the errors in the data are also important. It is not clear from existing data sets if errors are random or systematic, i.e. are phases systematically increased by near-surface scatter, or just randomly perturbed? The differences between the two cases is important in both the binning of the data [see (3)] and in computing the misfit of the data set to a given model.

(3) A likely experiment would utilize of the order of 10 receiver instruments. However, with a moving transmitter, it is quite possible that data will be transmitted from 1000 distinct locations. The computation required to model this is prohibitive, so data is binned by transmitter location, i.e. all signals transmitted from locations within say 500 m of a point are averaged as if they came from that single point. This reduces the number of transmitter locations to be considered, and the averaging may reduce the errors in the data. However, some knowledge of the statistics of the data errors is needed to avoid introducing artefacts into the data [see (2)].

With consideration of these factors, an inversion study was undertaken for three of the fast-spreading mid-ocean-ridge conductivity models that were considered in the forward modelling study of Unsworth (1994). These models are shown in the top row of Fig. 5 (opposite page 165), and in each the

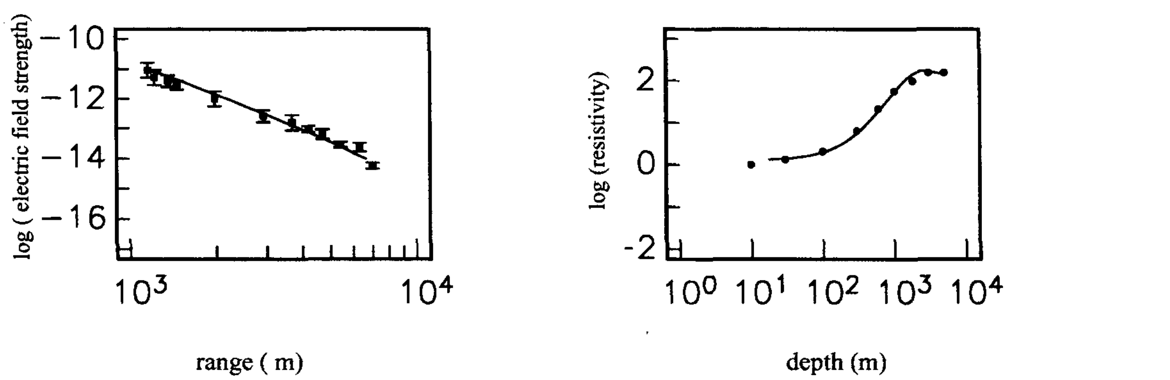

Figure 4. Results of inverting 8 Hz CSEM data collected over the East Pacific Rise in 1989. The left-hand panel shows the electric field strength with standard errors along with the response of the best-fitting smooth conductivity model. This model is shown by the solid curve in the right-hand panel, and is compared with the result of a 1-D inversion (circles) by Evans *et al.* (1994).

background conductivity model is the same with a 1 km thick Layer 2 with conductivity $0.01\,\mathrm{s\,m^{-1}}$ underlain by a more resistive, $0.001\,\mathrm{S\,m^{-1}}$, Layer 3. In model ML, a thin melt lens is present at the depth suggested by the seismic reflection study of Harding *et al.* (1989). The melt lens is 100 m thick and has a conductivity of $1\,\mathrm{S\,m^{-1}}$. In model MC, a low-melt-fraction magma chamber is present with a conductivity of $0.05\,\mathrm{S\,m^{-1}}$ and extends to the Moho at 6 km depth. In the third model, MC + HT, an active hydrothermal system is present, resulting in a more conductive Layer 2 above the magma body, and providing a conductive path from the ocean to the magma chamber.

The first set of inversions used data generated with transmitter and receiver dipoles parallel to the MOR. The geometry of the electromagnetic fields is analogous to the transverse electric (TE) mode in magnetotellurics. Receiver instruments were placed 1 km apart across the ridge, and a transmitter was deployed at each receiver location. The synthetic data were contaminated with 5 per cent random errors and then inverted for the smoothest conductivity model that fits the data. The data were fitted to a confidence level of 5 per cent, giving $\Phi_d = 1$. The inversion used the set of 88 vectors whose validity was justified in the previous section by comparison with traditional inversion methods. The resulting models are shown in the second row of Fig. 5. In each case the conductive Layer 2 is well resolved. Model ML clearly shows the melt lens, and the data from model MC shows the top of the conductive magma chamber, although its conductive base is not clearly imaged. Data from MC + HT clearly show the presence of a conductive hydrothermal zone extending from the melt body to the sea-floor. The lack of resolution of the resistive zone beneath the magma chamber is due to the fact that the dominant current flow is parallel to the ridge. The minor asymmetry of the models is due to the asymmetry of the noise added to the data.

The next set of inversions considers data in the same configuration as in the previous example, but with 10 per cent random errors added. The data were fitted to a confidence level of 10 per cent with $\Phi_d = 1$. Most of the features resolved at the 5 per cent error level are still resolved. The ML model can be distinguished from MC, and the presence of the hydrothermal zone, HT, is still discernible. However, the models have become significantly blurred.

In many electromagnetic exploration techniques, it is necessary to use orthogonal transmitters to image conductivity structures fully. This is true both for plane-wave sources, such as MT, and also for dipolar transmitters. Thus the next set of inversions uses dipoles oriented across the ridge and is analogous to the transverse magnetic (TM) mode in magnetotellurics. Data generated in this configuration will have electric fields in only the *y*-direction at the receivers. Synthetic data for this configuration were computed for the three conductivity models, and 5 per cent errors were added. The E_y data were inverted and the results are shown on the 4th row of Fig. 5. As before, the layered earth is imaged, and features in the upper 2 km of each model are distinct. This configuration produces a much clearer image of the lower crust, with the conductive–resistive transition at the base of the magma chamber being imaged. This is possible since significant electric current is crossing the base of the chamber, and the charge accumulation produces electric fields that are detectable at the surface. These effects are weaker than those in the dipole-parallel configuration, as is shown by a set of inversions at the 10 per cent uncertainty level in the next row of models. Neither the melt lens nor the magma chamber is imaged and only a near-surface conductor such as the hydrothermal zone produces fields that are detectable above a 10 per cent error level.

Electromagnetic exploration methods use signals that are diffusive in nature, and thus they are poor at resolving sharp interfaces, but good at determining the bulk properties of a region. Thus it is meaningful to consider how an electromagnetic technique might be combined with a seismic reflection survey to produce a clearer image of a mid-ocean ridge. The final set of inversions simulates a combined seismic–electromagnetic experiment in which the seismic reflection indicates that a sharp interface is located at 1.2 km depth beneath the sea-floor at the ridge crest. The E_y data with 10 per cent errors are inverted again, except that the weighting matrix, $\mathbf{W}_m$, is chosen so that the conductivity model is allowed to be discontinuous where a sharp seismic reflection is observed. This permits the high conductivity of the ML to be resolved. The inversion of data for model MC shows the true value of conductivity beneath the interface, but the deeper structure is poorly resolved for reasons discussed above. In the presence of a hydrothermal zone, the discontinuity allows the deeper structure to be well resolved.

To apply the results of this inversion study to the design of a real experiment, it is necessary to consider the factors (1)–(3) discussed above. The magnitude of errors to be expected in such data is one of the largest unknowns. In the presence of rugged topography or strong near-surface conductivity variations (e.g. at a slow-spreading ridge) these effects could be very large, and very limited structural information would be obtained. The distortion of the data would hide responses from deeper conductivity structure. Using many transmitter locations to average out this geological noise might help, but would require a huge set to be collected. It is highly likely that the distortion is 3-D in which case the problem might not be tractable.

The existent data and the calculations of Unsworth (1994) indicate that data with uncertainties in the 10–30 per cent range might be acquired in a region of relatively flat sea-floor, such as at a fast-spreading mid-ocean ridge. Limited spatial aliasing of the data would enable a CSEM technique to serve as a useful tool for studying mid-ocean-ridge crustal structure. A range of conductivity models could be distinguished, and the distribution of hydrothermal fluids and partial melt within the crust could be constrained.

ACKNOWLEDGMENTS

MJU gratefully acknowledges the support of a Killam Post-Doctoral Fellowship of the University of British Columbia. Computation was made possible at the UBC Geophysical Inversion Facility by NSERC Grant 5-84270, and also at the Geophysics Program, University of Washington, under DOE grant DE-FG06-92ER14231. The manuscript benefitted from reviews by Steve Constable and an anonymous reviewer.

REFERENCES

Chave, A.D., Edwards, R.N. & Constable, S.C., 1990. Electrical exploration methods for the seafloor, in *Electromagnetic methods in*

applied geophysics, Vol. 2, ed. Nabighian, M.N., Society of Exploration Geophysicists, Tulsa, OK.
deGroot-Hedlin, C. & Constable, S.C., 1990. Occam inversion to generate smooth two-dimensional resistivity models from magnetotelluric data, *Geophysics,* **55,** 1613–1624.
Evans, R.L., Sinha, M.C., Constable, S.C. & Unsworth, J.J., 1994. On the electrical nature of the axial melt zone at 13°N on the East Pacific Rise, *J. Geophys. Res.,* **B1,** 577–588.
Harding, A.J., Orcutt, J.A., Kappus, M.E., Vera, E.E., Mutter, J.C., Buhl, P., Detrick, R.S. & Brocher, T.M., 1989. Structure of young oceanic crust at 13°N on the East Pacific Rise from expanding spread profiles, *J. Geophys. Res.,* **94,** 12 163–12 196.
Kennett, B.L.N. & Williamson, P.R., 1988. Subspace methods for large-scale nonlinear inversion, in *Mathematical geophysics: a survey of recent developments in seismology and geodynamics,* pp. 139–154, eds Vlaar, N.J., Nolet, G., Wortel, M.J.R. & Cloetingth, S.A., D. Reidel, Dordrecht.
Lee, K.H. & Xie, G., 1993. A new approach to imaging with low frequency electromagnetic fields. *Geophysics,* **58,** 780–796.
McGillivray, P.R., Oldenburg, D.W. & Ellis, R.G., 1994. Calculation of sensitivities for the frequency domain electromagnetic induction problem, *Geophys. J. Int.,* **116,** 1–4.
Newman, G.A, 1992. Electromagnetic inversion using integral equations, *Abstract 11th Workshop on Electromagnetic Induction in the Earth,* Int. Assoc. of Geomagnetism and Aeronomy, August 1992, Wellington, N.Z.
Oldenburg, D.W., McGillivray, P.R. & Ellis, R.G., 1993. General subspace methods for large scale inverse problems, *Geophys. J. Int.,* **114,** 12–20.
Oristaglio, M.L. & Worthington, M.H., 1980. Inversion of surface and borehold electromagnetic data for two-dimensional electrical conductivity models, *Geophysical Prospect,* **28,** 633–657.
Skilling, J. & Bryan, R.K., 1984. Maximum entropy image reconstruction: general algorithm, *Mon. Not. R. astr. Soc.,* **211,** 111–124.
Smith, J.T. & Booker, J.R., 1988. Magnetotelluric inversion for minimum structure, *Geophysics,* **53,** 1565–1576.
Torres-Verdin, C. & Habashy, T.M., 1993. Cross well electromagnetic tomography, *Expanded abstract, 3rd Int. Congress of the Brazilian Geophysical Society. Rio de Janeiro, April 1993.*
Unsworth M.J., 1994. Exploration of mid-ocean ridges with a frequency domain electromagnetic system, *Geophys. J. Int.,* **116,** 447–467.
Unsworth, M.J., Travis, B.J. & Chave, A.D., 1993. Electromagnetic induction by a finite electric dipole source over a two-dimensional earth, *Geophysics,* **58,** 198–214.
Whittall, K.P. & Oldenburg, D.W., 1992. *Inversion of Magnetotelluric Data for a One-Dimensional Conductivity,* Geophys. Monograph Ser., No. 5, Soc. Expl. Geophys., Tulsa, OK.

APPENDIX A: SENSITIVITIES FOR $2\frac{1}{2}$-D PROBLEMS

The ith datum is a signal transmitted from a source S to a receiver R, as shown in Fig. A1. The sensitivity of this datum to the conductivity of the jth region, J_{ij}, can be computed by the adjoint method. McGillivray *et al.* (1994) show that it is given by

$$J_{ij} = \int_j \mathbf{E}^{\mathrm{S}} \cdot \mathbf{E}^{\mathrm{R}}\, d\mathbf{v}, \tag{A1}$$

where E_{S} is the electric field due to the actual source at S, and E_{R} is the field due to a source dipole of unit moment located at the receiver, R. Clearly, this method of computing the sensitivities requires that a forward modelling is carried out with a source at every receiver location. This computation is generally available, since arrays of instruments are considered in which data is generated by doing precisely this.

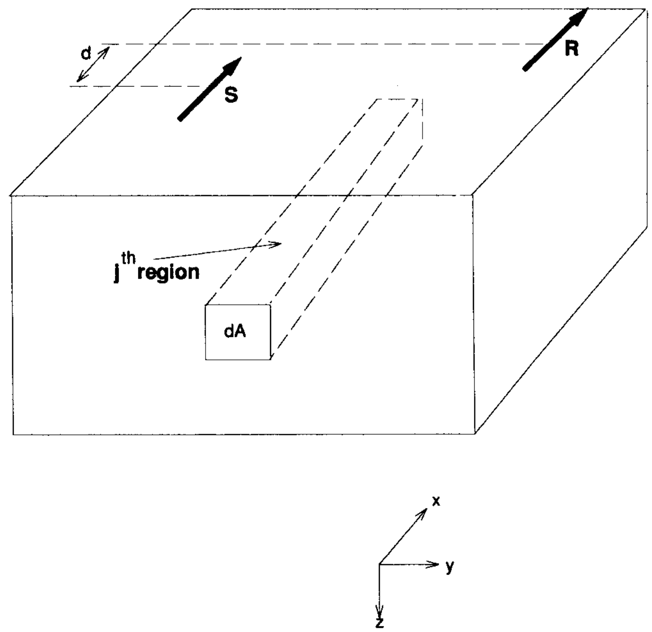

Figure A1. Geometry for the computation of adjoint sensitivities in the $2\frac{1}{2}$-D electromagnetic induction problem. The source (S) and receiver (R) dipoles are located on the Earth's surface. The conductivity of the Earth is parametrized in 2-D and is invariant in the x-direction.

In the $2\frac{1}{2}$-D problem, we calculate the sensitivity of the electric field transmitted from source (S) to receiver (R) to the conductivity of the prism (P). From McGillivray *et al.* (1994) this is given by

$$S = \int_{A_j} \int_{-\infty}^{\infty} \mathbf{E}_{\mathrm{S}} \cdot \mathbf{E}_{\mathrm{R}}\, dA\, dx. \tag{A2}$$

The electric fields are computed in the (k_x, y, z) domain, and thus

$$\mathbf{E}_{\mathrm{S}}(\mathbf{x}, \mathbf{y}, \mathbf{z}) = \frac{1}{2\pi} \int_{-\infty}^{\infty} \hat{\mathbf{E}}_{\mathrm{S}} \exp(-ik_{1x}x)\, dk_{1x}, \tag{A3}$$

$$\mathbf{E}_{\mathrm{R}}(\mathbf{x}, \mathbf{y}, \mathbf{z}) = \frac{1}{2\pi} \int_{-\infty}^{\infty} \hat{\mathbf{E}}_{\mathrm{S}} \exp(-ik_{2x}x)\, dk_{2x}, \tag{A4}$$

where the hat denotes a quantity in the Fourier transform domain. If we define the area integral of the two electric fields as

$$\int_A \hat{\mathbf{E}}_{\mathrm{S}}(k_{1x})\hat{\mathbf{E}}_{\mathrm{R}}(k_{2x})\, dA = \tilde{\mathbf{E}}(k_{1x}, k_{2x}), \tag{A5}$$

then it can be shown that

$$S = \frac{1}{4\pi^2} \int_x \int_{k_{1x}} \int_{k_{2x}} \tilde{E}(k_{1x}, k_{2x}) \times \exp[-i(k_{1x} + k_{2x})] \exp(-ik_{2x}d)\, dk_{1x}\, dk_{2x}\, dx, \tag{A6}$$

where d is the offset in the x-direction between source and receiver. Integrating over x and noting that

$$\delta(k_x) = \frac{1}{2\pi} \int \exp(-ik_x x)\, dx, \tag{A7}$$

where δ is the Dirac delta function, gives

$$S = \frac{1}{2\pi} \int_{k_{1x}} \int_{k_{2x}} \tilde{E}(k_{1x}, k_{2x}) \delta(k_{1x}, k_{2x}) \times \exp(-ik_{2x})\, dk_{1x}\, dk_{2x}. \quad \text{(A8)}$$

Integration over k_{x1} simplifies the result to

$$S = \frac{1}{2\pi} \int_{k_{x2}} \tilde{E}(-k_{2x}, k_{2x}) \exp(-ik_{2x}d)\, dk_{2x}. \quad \text{(A9)}$$

When the dipole is parallel to the x-direction, the term $E_{Sx}(-k_x)E_{Rx}(k_x)$ will be symmetric in k_x, and $E_{Sy}(-k_x)E_{Ry}(k_x)$ and $E_{Sz}(-k_x)E_{rz}(k_x)$ will be antisymmetric in k_x. Thus the sensitivity is given by

$$S = \frac{1}{\pi} \int_{k_x=0}^{k_x=\infty} \tilde{E}(k_x, k_x) \cos(k_x d)\, dk_x. \quad \text{(A10)}$$